



1

2

3

4

5 **Speciated atmospheric mercury and sea-air exchange of**
6 **gaseous mercury in the South China Sea**

7

8

9 Chunjie Wang¹, Zhangwei Wang¹, Fan Hui², Xiaoshan Zhang¹

10

11

12

13

14

15 ¹ Research Center for Eco-Environmental Sciences, Chinese Academy of Sciences, 18 Shuangqing Road, Beijing,

16 China

17 ² China University of Petroleum (Beijing), 18 Fuxue Road, Beijing, China

18

19

20

21

22 Correspondence to: Xiaoshan Zhang (zhangxsh@rcees.ac.cn)

23

24

25

26

27

28

29

30

31

32

33

34

35



36 Abstract

37 The characteristics of the reactive gaseous mercury (RGM) and particulate mercury (Hg^{P}) in the
38 marine boundary layer (MBL) is poorly understood due in part to sparse data from sea and ocean.
39 Gaseous elemental Hg (GEM), RGM and size-fractioned Hg^{P} in marine atmosphere, and dissolved
40 gaseous Hg (DGM) in surface seawater were determined in the South China Sea (SCS) during an
41 oceanographic expedition (3–28 September 2015). The mean concentrations of GEM, RGM and
42 $\text{Hg}^{\text{P}}_{2.5}$ were $1.52 \pm 0.32 \text{ ng m}^{-3}$, $6.1 \pm 5.8 \text{ pg m}^{-3}$ and $3.2 \pm 1.8 \text{ pg m}^{-3}$, respectively. Low GEM
43 level indicated that the SCS suffered less influence from human activities, which could be due to
44 the majority of air masses coming from the open oceans as modeled by backward trajectories.
45 Atmospheric reactive Hg (RGM + $\text{Hg}^{\text{P}}_{2.5}$) represented less than 1 % of total atmospheric Hg,
46 indicating that atmospheric Hg existed mainly as GEM in the MBL. The GEM and RGM
47 concentrations in the northern SCS were significantly higher than those in the western SCS, and
48 the $\text{Hg}^{\text{P}}_{2.5}$ and $\text{Hg}^{\text{P}}_{10}$ levels in the Pearl River Estuary were significantly higher than those in the
49 open waters of the SCS, indicating that the Pearl River Estuary was polluted to some extent. The
50 size distribution of Hg^{P} in PM_{10} was observed to be bi-modal with a higher peak (5.8–9.0 μm) and
51 a lower peak (0.7–1.1 μm), but the coarse modal was the dominant size, especially in the open
52 SCS. There was no significant diurnal variation of GEM and $\text{Hg}^{\text{P}}_{2.5}$, but we found the RGM
53 concentrations were significantly higher in daytime than in nighttime mainly due to the influence
54 of solar radiation. In the northern SCS, the DGM concentrations in nearshore areas were higher
55 than those in the open sea, but this pattern was not significant in the western SCS. The sea-air
56 exchange fluxes of Hg^0 in the SCS varied from 0.40 to $12.71 \text{ ng m}^{-2} \text{ h}^{-1}$ with a mean value of 4.99
57 $\pm 3.32 \text{ ng m}^{-2} \text{ h}^{-1}$. The annual emission flux of Hg^0 from the SCS to the atmosphere was estimated
58 to be $159.6 \text{ tons yr}^{-1}$, accounting for about 5.54 % of the global Hg^0 oceanic evasion though the
59 SCS only represents 1.0 % of the global ocean area. Additionally, the annual dry deposition flux of
60 atmospheric reactive Hg represented more than 18 % of the annual evasion flux of Hg^0 , and
61 therefore the dry deposition of atmospheric reactive Hg was an important pathway for the input of
62 atmospheric Hg to the SCS.

63 1 Introduction

64 Mercury (Hg) is a naturally occurring metal. Hg is released to the environment through both the
65 natural and anthropogenic pathways (Schroeder and Munthe, 1998). However, since the Industrial
66 Revolution, the anthropogenic emissions of Hg increased drastically. Continued rapid
67 industrialization has made Asia the largest source region of Hg emissions to air, with East and
68 Southeast Asia accounting for about 40 % of the global total (UNEP, 2013). Three operationally
69 defined Hg forms are present in the atmosphere: gaseous elemental Hg (GEM or Hg^0), reactive
70 gaseous Hg (RGM) and particulate Hg (Hg^{P}) (Schroeder and Munthe, 1998; Landis et al., 2002),
71 while they have different physicochemical characteristics. GEM is very stable with a residence



72 time of 0.2–1 yr due to its high volatility and low solubility (Weiss-Penzias et al., 2003; Radke et
73 al., 2007; Selin et al., 2007; Horowitz et al., 2017). Therefore, GEM can be transported for a
74 long-range distance in the atmosphere, and this makes it well-mixed on a regional and global scale.
75 Generally, GEM makes up more than 95 % of total atmospheric Hg (TAM), while the RGM and
76 Hg^P concentrations (collectively known as atmospheric reactive mercury) are typically 2–3 orders
77 of magnitude smaller than GEM in part because they are easily removed from ambient air by wet
78 and dry deposition (Laurier and Mason, 2007; Holmes et al., 2009; Gustin et al., 2013), and they
79 can also be reduced back to Hg⁰.

80 Numerous previous studies have shown that Hg⁰ in the marine boundary layer (MBL) can be
81 rapidly oxidized to form RGM in situ (Hedgecock et al., 2003; Laurier et al., 2003; Sprovieri et al.,
82 2003, 2010; Laurier and Mason, 2007; Soerensen et al., 2010a; Wang et al., 2015). Ozone and OH
83 could potentially be important oxidants on aerosols (Ariya et al., 2015), while the reactive halogen
84 species (e.g., Br, Cl and BrO, generating from sea salt aerosols) may be the dominant sources for
85 the oxidation of Hg⁰ in the MBL (Laurier et al., 2003; Sander et al., 2003; Holmes et al., 2006,
86 2010; Seigneur and Lohman, 2008; Auzmendi-Murua et al., 2014; Gratz et al., 2015; Steffen et al.,
87 2015; Shah et al., 2016; Horowitz et al., 2017). The wet and dry deposition (direct or uptake by
88 sea-salt aerosol) represents a major input of RGM and Hg^P to the sea and ocean due to their
89 special and unique characteristics (i.e., high reactivity and water solubility) (Lindberg and Stratton,
90 1998; Landis et al., 2002; Mason and Sheu, 2002; Holmes et al., 2009). Previous studies also
91 showed that atmospheric wet and dry deposition of RGM (mainly HgBr₂, HgCl₂, HgO,
92 Hg-nitrogen and sulfur compounds) was the greatest source of Hg to open oceans (Mason and
93 Sheu, 2002; Holmes et al., 2009; Mason et al., 2012; Huang et al., 2017). A recent study suggested
94 that approximately 80 % of atmospheric reactive Hg sinks into the global oceans, and most of the
95 deposition takes place to the tropical oceans (Horowitz et al., 2017).

96 The atmospheric reactive Hg deposited to the oceans follows different reaction pathways, and
97 one important process is that divalent Hg can be combined with the existing particles followed by
98 sedimentation, or be converted to methylmercury (MeHg), the most bioaccumulative and toxic
99 form of Hg in seafood (Ahn et al., 2010; Mason et al., 2017), another important process is that the
100 divalent Hg can be converted to dissolved gaseous Hg (DGM) through abiotic and biotic
101 mechanisms (Fitzgerald et al., 2007; Strode et al., 2007). It is well known that almost all DGM in
102 the surface seawater is Hg⁰ (Mason et al., 1995; Horvat et al., 2003), while the dimethylmercury is
103 extremely rare in the surface seawater (Hammerschmidt et al., 2012; Bowman et al., 2015). It has
104 been found that a majority of the surface seawater was supersaturated with respect to Hg⁰
105 (Fitzgerald et al., 2007; Soerensen et al., 2010b, 2013, 2014), and parts of this Hg⁰ may be emitted
106 to the atmosphere. Evasion of Hg⁰ from the oceanic surface into the atmosphere is partly driven by
107 the solar radiation and aquatic Hg pools of natural and anthropogenic origins (Andersson, et al.,
108 2011). Sea-air exchange is an important component of the global Hg cycle as it mediates the rate



109 of increase in ocean Hg and therefore the rate of change in level of MeHg. Consequently, Hg⁰
110 evasion from sea surface not only decreases the amount of Hg available for methylation in waters
111 but also has an important effect on the redistribution of Hg in the global environment (Mason and
112 Sheu, 2002; Strode et al., 2007).

113 In recent years, speciated atmospheric Hg has been monitored in coastal areas (e.g., Choi et
114 al., 2008; Cheng et al., 2013, 2014; Xu et al., 2015; Mao et al., 2016; Howard et al., 2017) and
115 open seas and oceans (e.g., Laurier and Mason, 2007; Chand et al., 2008; Soerensen et al., 2010a;
116 Wang et al., 2016a, b). However, there exists a dearth of knowledge regarding speciated
117 atmospheric Hg and sea-air exchange of Hg⁰ in tropical seas, such as the South China Sea (SCS).
118 The highly time-resolved ambient GEM concentrations were measured using a Tekran[®] system.
119 Simultaneously, the RGM, Hg^P and DGM were measured using manual methods. The main
120 objectives of this study are to identify the spatial-temporal characteristics of speciated atmospheric
121 Hg and to investigate the DGM concentrations in the SCS during the cruise, and then to calculate
122 the Hg⁰ flux based on the meteorological parameters as well as the concentrations of GEM in air
123 and DGM in surface seawater. These results will raise our knowledge of the Hg cycle in tropical
124 marine atmosphere and waters.

125 2 Materials and methods

126 2.1 Study area

127 The SCS is located in the downwind of Southeast Asia (Fig. 1a), and it is the largest semi-enclosed
128 marginal sea in the western tropical Pacific Ocean. The SCS is connected with the East China Sea
129 (ECS) to the northeast and the western Pacific Ocean to the east (Fig. 1a). The SCS is surrounded
130 by numerous developing and developed countries (see Fig. 1a). An open cruise was organized by
131 the South China Sea Institute of Oceanology (Chinese Academy of Sciences) and conducted
132 during the period of 3–28 September 2015. The sampling campaign was conducted on R/V *Shiyan*
133 3, which departed from Guangzhou, circumnavigated the northern and western SCS and then
134 returned to Guangzhou. The DGM sampling stations and R/V tracks are plotted in Fig. 1b. In this
135 study, meteorological parameters (including photosynthetically available radiation (PAR)
136 (Li-COR[®], Model: Li-250), wind speed, air temperature and RH) were measured synchronously
137 with atmospheric Hg onboard the R/V.

138 2.2 Experimental methods

139 2.2.1 Atmospheric GEM measurements

140 In this study, GEM was measured using an automatic dual channel, single amalgamation cold
141 vapor atomic fluorescence analyzer (Model 2537B, Tekran[®], Inc., Toronto, Canada), which has
142 been reported in our previous studies (Wang et al., 2016a, b, c). In order to reduce the



143 contamination from ship exhaust plume as possible, we installed the Tekran[®] system inside the
144 ship laboratory (the internal air temperature was controlled to 25 °C using an air conditioner) on
145 the fifth deck of the R/V and mounted the sampling inlet at the front deck 1.5 m above the top
146 deck (about 16 m above sea level) using a 7 m heated (maintained at 50 °C)
147 polytetrafluoroethylene (PTFE) tube (¼ inch in outer diameter). The sampling interval was 5 min
148 and the air flow rate was 1.5 l min⁻¹ in this study. Moreover, two PTFE filters (0.2 µm pore size,
149 47 mm diameter) were positioned before and after the heated line, and the soda lime before the
150 instrument was changed every 3 days during the cruise. The Tekran[®] instrument was calibrated
151 every 25 h using the internal calibration source and these calibrations were checked by injections
152 of certain volume of saturated Hg⁰ before and after this cruise. The relative percent difference
153 between manual injections and automated calibrations was < 5 %. The precision of the analyzer
154 was determined to > 97 %, and the detection limit was < 0.1 ng m⁻³.

155 The meteorological and basic seawater parameters were collected onboard the R/V, which
156 was equipped with meteorological and oceanographic instrumentations. To investigate the
157 influence of air masses movements on the GEM levels, 72-h backward trajectories of air masses
158 were calculated using the Hybrid Single Particle Lagrangian Integrated Trajectory (HYSPPLIT)
159 model (Draxler and Rolph, 2012) and TrajStat software (Wang et al., 2009) based on Geographic
160 Information System. Global Data Assimilation System (GDAS) meteorological dataset
161 (<ftp://arlftp.arlhq.noaa.gov/pub/archives/gdas1/>) with 1° × 1° latitude and longitude horizontal
162 spatial resolution and 23 vertical levels at 6-h intervals was used as the HYSPPLIT model input. It
163 should be noted that the start time of each back trajectory was identical to the GEM sampling time
164 (UTC) and the start height was 500 m above sea level.

165 2.2.2 Sampling and analysis of RGM and Hg^P

166 The Hg^P_{2.5} (Hg^P in PM_{2.5}) was collected on quartz filter (47 mm in diameter, Whatman), which has
167 been reported in several previous studies (Landis et al., 2002; Liu et al., 2011; Kim et al., 2012;).
168 It should be pointed out that the KCl coated denuders were heated at 500 °C for 1 h and the quartz
169 filters were pre-cleaned by pyrolysis at 900 °C for 3 h to remove the possible pollutant. The RGM
170 and Hg^P_{2.5} were sampled using a manual system (URG-3000M), which has been reported in
171 previous studies (Landis et al., 2002; Liu et al., 2011; Wang et al., 2016b). The sampling unit
172 includes an insulated box (Fig. S1), two quartz annular denuders, two Teflon filter holder (URG
173 Corporation) and a pump etc. The sampling flow rate was 10 l min⁻¹ (Landis et al., 2002), and the
174 sampling inlet was 1.2 m above the top deck of the R/V. In this study, one Hg^P_{2.5} sample was
175 collected in the daytime (6:00–18:00) and the other in the nighttime (18:00–6:00 (next day)),
176 while two RGM samples were collected in the daytime (6:00–12:00 and 12:00–18:00, local time)
177 and one RGM sample in the nighttime. Quality assurance and quality control for Hg^P and RGM
178 were carried out using field blank samples and duplicates. The field blank denuders and quartz



179 filters were treated similarly to the other samples but not sampling. The mean relative differences
180 of duplicated $\text{Hg}^{\text{P}}_{2.5}$ and RGM samples ($n = 6$) were $13 \pm 6 \%$ and $9 \pm 7 \%$, respectively.

181 Meanwhile, we collected different size particles using an Andersen impactor (nine-stage),
182 which has been widely used in previous studies (Feddersen et al., 2012; Kim et al., 2012; Zhu et
183 al., 2014; Wang et al., 2016a). The Andersen cascade impactor was installed on the front top deck
184 of the R/V to sample the size-fractioned particles in PM_{10} . In order to diminish the contamination
185 from exhaust plume of the ship as much as possible, we turned off the pump when R/V arrived at
186 stations, and then switched back on when the R/V went to next station. The sample collection
187 began in the morning (10:00 am) and continued for 2 days with a sampling flow rate of 28.3 l
188 min^{-1} . Field blanks for Hg^{P} were collected by placing nine pre-cleaned quartz filters (81 mm in
189 diameter, Whatman) in another impactor for 2 days without turning on the pump. After sampling,
190 the quartz filters were placed in cleaned plastic boxes (sealing in Zip Lock plastic bags), and then
191 were immediately preserved at $-20 \text{ }^{\circ}\text{C}$ until the analysis.

192 The detailed analysis processes of RGM and Hg^{P} have been reported in our previous studies
193 (Wang et al., 2016a, b). Briefly, the denuder and quartz filter were thermally desorbed at $500 \text{ }^{\circ}\text{C}$
194 and $900 \text{ }^{\circ}\text{C}$, respectively, and then the resulting thermally decomposed Hg^0 in carrier gas (zero air,
195 i.e., Hg-free air) was quantified. The method detection limit was calculated to be 0.67 pg m^{-3} for
196 RGM based on 3 times the standard deviation of the blanks ($n = 57$) for the whole dataset. The
197 average field blank of denuders was $1.2 \pm 0.6 \text{ pg}$ ($n = 6$). The average blank values ($n = 6$) of
198 $\text{Hg}^{\text{P}}_{2.5}$ and $\text{Hg}^{\text{P}}_{10}$ were 1.4 pg (equivalent of $< 0.2 \text{ pg m}^{-3}$ for a 12 h sampling time) and 3.2 pg
199 (equivalent of $< 0.04 \text{ pg m}^{-3}$ for a 2-day sampling time) of Hg per filter, respectively. The
200 detection limits of $\text{Hg}^{\text{P}}_{2.5}$ and $\text{Hg}^{\text{P}}_{10}$ were all less than 1.5 pg m^{-3} based on 3 times the standard
201 deviation of field blanks. It should be noted that the average field blanks for RGM and Hg^{P} were
202 subtracted from the samples.

203 2.2.3 Determination of DGM in surface seawater

204 In this study, the analysis was carried out according to the trace element clean technique, all
205 containers (borosilicate glass bottles and PTFE tubes, joints and valves) were cleaned prior to use
206 with detergent, followed by trace-metal-grade HNO_3 and HCl , and then rinsed with Milli-Q water
207 ($> 18.2 \text{ M}\Omega \text{ cm}^{-1}$), which has been described in our previous study (Wang et al., 2016c). DGM
208 were measured in situ using a manual method (Fu et al., 2010; Ci et al., 2011). The detailed
209 sampling and analysis of DGM has been elaborated in our previous study (Wang et al., 2016c).
210 The analytical blanks were conducted onboard the R/V by extracting Milli-Q water for DGM. The
211 mean concentration of DGM blank was $2.3 \pm 1.2 \text{ pg l}^{-1}$ ($n = 6$), accounting for 3–10 % of the raw
212 DGM in seawater samples. The method detection limit was 3.6 pg l^{-1} on the basis of three times
213 the standard deviation of system blanks. The relative standard deviation of duplicate samples
214 generally $< 8 \%$ of the mean concentration ($n = 6$).



215 2.2.4 Estimation of sea-air exchange flux of Hg⁰

216 The sea-air flux of Hg⁰ was calculated using a thin film gas exchange model developed by Liss
217 and Slater (1974) and Wanninkhof (1992). The detailed calculation processes of Hg⁰ flux have
218 been reported in recent studies (Ci et al., 2011; Kuss, 2014; Wang et al., 2016c; Kuss et al., 2018).
219 It should be noted that the Schmidt number for gaseous Hg (Sc_{Hg}) is defined as the following
220 equation: $Sc_{Hg} = \nu/D_{Hg}$, where ν is the kinematic viscosity ($cm^2 s^{-1}$) of seawater calculated using
221 the method of Wanninkhof (1992), D_{Hg} is the Hg⁰ diffusion coefficient ($cm^2 s^{-1}$) in seawater,
222 which is calculated according to the recent research (Kuss, 2014). The degree of Hg⁰ saturation (S_a)
223 was calculated using the following equation: $S_a = H' DGM_{conc.}/GEM_{conc.}$, and the calculation of H'
224 (the dimensionless Henry's Law constant) has been reported in previous studies (Ci et al., 2011,
225 2015; Kuss, 2014).

226 3 Results and discussion

227 3.1 Speciated atmospheric Hg concentrations

228 Figure 2 shows the time series of speciated atmospheric Hg and meteorological parameters during
229 the cruise in the SCS. The GEM concentration during the whole study period ranged from 0.92 to
230 4.12 ng m⁻³ with a mean value of 1.52 ± 0.32 ng m⁻³ ($n = 4673$), which was comparable to the
231 average GEM level over the global open oceans (Soerensen et al., 2010a), and higher than those at
232 background sites in the Southern Hemisphere (Slemr et al., 2015; Howard et al., 2017), and also
233 higher than those in remote oceans, such as the Cape Verde Observatory station (Read et al., 2017),
234 the Atlantic Ocean (Laurier and Mason, 2007; Soerensen et al., 2013), the equatorial Pacific
235 Ocean (Soerensen et al., 2014) and the Indian Ocean (Witt et al., 2010; Angot et al., 2014), but
236 lower than those in marginal seas, such as the Bohai Sea (BS), Yellow Sea (YS) and East China
237 Sea (ECS) (Table 1). However, previous studies (Fu et al., 2010; Tseng et al., 2012) conducted in
238 the northern SCS showed that the average GEM concentrations in their study period (Fu et al.,
239 2010; Tseng et al., 2012) were higher than that in this study (Table 1). This is due to the fact that
240 the GEM level in the northern SCS (Fu et al., 2010; Tseng et al., 2012) were considerably higher
241 than that in the western SCS (this study).

242 The Hg^{P_{2,5}} concentrations over the SCS ranged from 1.2 to 8.3 pg m⁻³ with a mean value of
243 3.2 ± 1.8 pg m⁻³ ($n = 39$) (Fig. 2), which was higher than those observed at Nam Co (China) and
244 the Amsterdam Island, and were comparable to those in other coastal areas, such as the Okinawa
245 Island, the Nova Scotia, the Adriatic Sea, the Ontario lake and the Weeks Bay (see Table 1), but
246 lower than those in the BS and YS (Wang et al., 2016b), and considerably lower than those in
247 rural and urban sites, such as Xiamen, Seoul (see Table 1), Guiyang and Waliguan (Fu et al., 2011,
248 2012). The results showed that the SCS suffered less influence from human activities. The RGM
249 concentration over the SCS ranged from 0.27 to 27.57 pg m⁻³ with a mean value of 6.1 ± 5.8 pg



250 m^{-3} ($n = 58$), which was comparable to those in other seas, such as the North Pacific Ocean, the
251 North Atlantic Ocean and the Mediterranean Sea (including the Adriatic Sea) (Table 1), and higher
252 than the global mean RGM concentration in the MBL (Soerensen et al., 2010a), and also higher
253 than those measured at a few rural sites (Valente et al., 2007; Liu et al., 2010; Cheng et al., 2013,
254 2014), but significantly much lower than those polluted urban areas in China and South Korea,
255 such as Guiyang ($35.7 \pm 43.9 \text{ pg m}^{-3}$, Fu et al., 2011), Xiamen, and Seoul (Table 1). Furthermore,
256 Figure 2 shows that the long-lived GEM has smaller variability compared to the short-lived
257 species like RGM and $\text{Hg}^{\text{P}}_{2,5}$, indicating that atmospheric reactive Hg was easily scavenged from
258 the marine atmosphere due to their high activity and solubility. This pattern was consistent with
259 our previous observed patterns in the BS and YS (Wang et al., 2016b). Moreover, we found that
260 atmospheric reactive Hg represents less than 1 % of TAM in the atmosphere, which was
261 comparable to those measured in other marginal and inner seas, such as the BS and YS (Wang et
262 al., 2016b), Adriatic Sea (Sprovieri and Pirrone, 2008), Okinawa Island (located in the ECS)
263 (Chand et al., 2008), but was significantly lower than those at the urban sites (Table 1).

264 3.2 Spatial distribution of atmospheric Hg

265 3.2.1 Spatial distributions of GEM and RGM

266 The spatial distribution of GEM over the SCS is illustrated in Fig. 3a. The mean GEM
267 concentration in the northern SCS ($1.73 \pm 0.40 \text{ ng m}^{-3}$ with a range of 1.01–4.12 ng m^{-3}) was
268 significantly higher than that in the western SCS ($1.41 \pm 0.26 \text{ ng m}^{-3}$ with a range of 0.92–2.83 ng
269 m^{-3}) (t -test, $p < 0.01$). Additionally, we found that the GEM concentrations in the PRE (the
270 average value $> 2.00 \text{ ng m}^{-3}$) were significantly higher than those in the open SCS (see Figs. 2, 3a),
271 indicating that this nearshore area suffered from high GEM pollution in our study period probably
272 due to the surrounding human activities. Figure 3a shows that there was large difference in GEM
273 concentration between stations 1–10 and stations 16–31. The 72-h back-trajectories of air masses
274 showed that the air masses with low GEM levels between stations 1 and 10 mainly originated
275 from the SCS (Fig. S2a), while the air masses with high GEM levels at stations 16–31 primarily
276 originated from East China and ECS, and then passed over the southeast coastal regions of China
277 (Fig. S2b). Additionally, Fig. 3a shows that there was small variability of GEM concentrations
278 over the western SCS except the measurements near the station 79. The back-trajectories showed
279 that the air masses with elevated GEM level near the station 79 originated from the south of the
280 Taiwan Island, while the other air masses mainly originated from the West Pacific Ocean (Fig. S3a)
281 and the Andaman Sea (Fig. S3b). Therefore, the air masses dominantly originated from sea and
282 ocean in this study period, and this could be the main reason for the low GEM level over the SCS.
283 In conclusion, GEM concentrations showed a conspicuous dependence on the sources and
284 movement patterns of air masses during this cruise. In addition to the anthropogenic emissions, the
285 emission of Hg^0 from the surface seawater may be another important source of Hg^0 to the



286 atmosphere (Ci et al., 2011; Soerensen et al., 2013, 2014), especially for this tropical sea.

287 The spatial distribution of RGM over the SCS is plotted in Fig. 3b. The mean RGM
288 concentration in the northern SCS ($7.1 \pm 1.4 \text{ pg m}^{-3}$) was also obviously higher than that in the
289 western SCS ($3.8 \pm 0.7 \text{ pg m}^{-3}$) (*t*-test, $p < 0.05$), indicating that a portion of RGM in the northern
290 SCS maybe originated from the anthropogenic emission. We observed elevated RGM
291 concentrations in the PRE, and which was consistent with the GEM distribution pattern, indicating
292 that part of the RGM near PRE probably originated from the surrounding human activities. This is
293 confirmed by the following fact: The RGM concentrations in nighttime of the two days in the PRE
294 were 11.3 and 5.2 pg m^{-3} (Fig. S3), and they were significantly higher than those in the open SCS.
295 Another obvious feature is that the amplitude of RGM concentration is much greater than the
296 GEM, and this further indicated that the RGM was easily removed from the atmosphere through
297 both the wet and dry deposition. In addition, we found that the RGM concentrations in the
298 nearshore area were not always higher than those in the open sea except the measurements in the
299 PRE, suggesting that the RGM in the remote marine atmosphere presumably not originated from
300 land but from the in situ photo-oxidation of Hg^0 , which had been reported in previous studies (e.g.,
301 Hedgecock and Pirrone, 2001; Lindberg et al., 2002; Laurier et al., 2003; Sprovieri et al., 2003,
302 2010; Sheu and Mason, 2004; Laurier and Mason, 2007; Soerensen et al., 2010a; Wang et al.,
303 2015).

304 3.2.2 Spatial distributions of $\text{Hg}^{\text{P}}_{2.5}$ and $\text{Hg}^{\text{P}}_{10}$

305 The concentrations and spatial distribution of $\text{Hg}^{\text{P}}_{2.5}$ in the MBL are illustrated in Fig. 4a. The
306 highest $\text{Hg}^{\text{P}}_{2.5}$ value (8.3 pg m^{-3}) was observed in the PRE during daytime on 4 September 2015
307 presumably because of the local human activities. The homogeneous distribution and lower level
308 of $\text{Hg}^{\text{P}}_{2.5}$ in the open SCS indicated that the $\text{Hg}^{\text{P}}_{2.5}$ not originated from the land and the SCS
309 suffered less influence from human activities especially in the open sea. This is due to the fact that
310 the majority of air masses in the SCS during this study period came from the seas and oceans. The
311 spatial distribution pattern of $\text{Hg}^{\text{P}}_{2.5}$ in this study was different from our previous observed
312 patterns in the BS and YS (Wang et al., 2016b), which showed that $\text{Hg}^{\text{P}}_{2.5}$ concentrations in
313 nearshore area were higher than those in the open sea both in spring and fall mainly due to the
314 outflow of atmospheric Hg^{P} from East China.

315 The concentrations and spatial distributions of $\text{Hg}^{\text{P}}_{10}$ in the MBL of the SCS are illustrated in
316 Fig. 4b. We found that the $\text{Hg}^{\text{P}}_{10}$ concentration was considerably (2–7 times) higher in the PRE
317 than those of other regions of the SCS probably due to the large emissions of anthropogenic Hg in
318 surrounding areas of the PRE. Moreover, the highest $\text{Hg}^{\text{P}}_{2.1}/\text{Hg}^{\text{P}}_{10}$ ratio (41 %) was observed in the
319 PRE and coastal sea area of Hainan Island, while lowest ratio (22 %) was observed in the open sea
320 (Fig. 4b). The $\text{Hg}^{\text{P}}_{10}$ concentrations and $\text{Hg}^{\text{P}}_{2.1}/\text{Hg}^{\text{P}}_{10}$ ratios were higher in the nearshore area
321 compared to those in the open sea, demonstrating that coastal sea areas are polluted by



322 anthropogenic Hg to a certain extent. Interestingly, we found the mean $\text{Hg}^{\text{P}}_{2.1}$ concentration (3.16
323 $\pm 2.69 \text{ pg m}^{-3}$, $n = 10$) measured using the Andersen sampler was comparable to the mean $\text{Hg}^{\text{P}}_{2.5}$
324 concentration ($3.33 \pm 1.89 \text{ pg m}^{-3}$, $n = 39$) measured using a 47 mm Teflon filter holder (t -test, $p >$
325 0.1). This indicated that the fine Hg^{P} level in the MBL of the SCS was indeed low, and there might
326 be no significant difference in Hg^{P} concentration in the SCS between 12 h and 48 h sampling time.

327 The concentrations of all size-fractionated Hg^{P} are summarized in Table S1. The size
328 distribution of Hg^{P} in the MBL of the SCS is plotted in Fig. 5. One striking feature is that the
329 bi-modal pattern (a higher peak (5.8–9.0 μm) and a lower peak (0.7–1.1 μm)) was observed for
330 the size distributions of Hg^{P} in the open sea (Fig. 5a) if we excluded the data in the PRE. The
331 bi-modal pattern was more obvious when we consider all the data (Fig. 5b). Generally, the Hg^{P}
332 concentrations in coarse particles were significantly higher than those in fine particles, and $\text{Hg}^{\text{P}}_{2.1}$
333 contributed approximately 32 % (22–41 %, see Fig. 4b) to the $\text{Hg}^{\text{P}}_{10}$ for the whole data, indicating
334 that the coarse mode was the dominant size during this study period. This might be explained by
335 the sources of the air masses. Since air masses dominantly originated from sea and ocean (Figs. S1,
336 S2) and contained high concentrations of sea salts which generally exist in the coarse mode (1–10
337 μm) (Athanasopoulou et al., 2008; Mamane et al., 2008), the $\text{Hg}^{\text{P}}_{2.1}/\text{Hg}^{\text{P}}_{10}$ ratios were generally
338 lower in the SCS compared to those in the BS, YS and ECS (Wang et al., 2016a).

339 3.3 Dry deposition fluxes of RGM and Hg^{P}

340 The dry deposition flux of $\text{Hg}^{\text{P}}_{10}$ was obtained by summing the dry deposition fluxes of each
341 size-fractionated Hg^{P} in the same set. The dry deposition flux of $\text{Hg}^{\text{P}}_{10}$ is calculated using the
342 following equation: $F = \sum \text{CHg}^{\text{P}} \times V_{\text{d}}$, the F is the dry deposition flux of $\text{Hg}^{\text{P}}_{10}$ ($\text{ng m}^{-2} \text{d}^{-1}$), CHg^{P}
343 is the concentration of Hg^{P} in each size fraction (pg m^{-3}), and V_{d} is the corresponding dry
344 deposition velocity (cm s^{-1}). In this study, the dry deposition velocities of 0.03, 0.01, 0.06, 0.15
345 and 0.55 cm s^{-1} (Giorgi, 1988; Pryor et al., 2000; Nho-Kim et al., 2004) were chosen for the
346 following size-fractionated particles: < 0.4 , 0.4–1.1, 1.1–2.1, 2.1–5.8 and 5.8–10 μm , respectively
347 (Wang et al., 2016a). The average dry deposition flux of $\text{Hg}^{\text{P}}_{10}$ was estimated to be $1.08 \text{ ng m}^{-2} \text{d}^{-1}$
348 based on the average concentrations of each size-fractionated Hg^{P} in the SCS (Table S2), which
349 was lower than those in the BS, YS and ECS (Wang et al., 2016a). The dry deposition velocity of
350 RGM was 4.0–7.6 cm s^{-1} because of its characteristics and rapid uptake by sea salt aerosols
351 followed by deposition (Poissant et al., 2004; Selin et al., 2007). The annual dry deposition fluxes
352 of $\text{Hg}^{\text{P}}_{10}$ and RGM to the SCS were calculated to be 1.42 and 27.39–52.05 tons yr^{-1} based on the
353 average $\text{Hg}^{\text{P}}_{10}$ and RGM concentrations and the area of the SCS ($3.56 \times 10^{12} \text{ m}^2$). The result
354 showed that RGM contributed more than 95 % to the total dry deposition of atmospheric reactive
355 Hg. The annual dry deposition flux of RGM was considerably higher than that of the $\text{Hg}^{\text{P}}_{10}$ due to
356 the higher deposition rate and concentrations of RGM.

357 3.4 Temporal variation of atmospheric Hg



358 3.4.1 diurnal variation of GEM

359 The diurnal variation of GEM concentration during the whole study period is illustrated in Fig. 6.
360 It was notable that there was no significant variability of the mean (\pm SD) GEM concentration in a
361 whole day during this study period, and the GEM concentration dominantly fell in the range of
362 1.3–1.7 ng m⁻³ (Fig. 6). The statistical result showed that the mean GEM concentration in the
363 daytime (6:00–18:00) (1.49 ± 0.06 pg m⁻³) was comparable to that in the nighttime (1.51 ± 0.06
364 pg m⁻³) (*t*-test, $p > 0.05$). The lower GEM concentrations and smaller variability over the SCS
365 further revealed that the SCS suffered less influence of human activities, and the evasion of DGM
366 in local or regional surface seawater of the SCS and surrounding oceans was probably an
367 important source for the GEM in the marine atmosphere.

368 3.4.2 Daily variation of RGM

369 The average RGM concentrations in the daytime and nighttime are illustrated in Fig. 7. Firstly, it
370 could be found that RGM showed a diurnal variation with higher concentrations in the daytime
371 and lower concentrations in the nighttime during the whole study period. The mean RGM
372 concentration in the daytime (8.0 ± 5.5 pg m⁻³) was significantly and considerably higher than that
373 in the nighttime (2.2 ± 2.7 pg m⁻³) (*t*-test, $p < 0.001$). This diurnal pattern was in line with the
374 previous multiple sites studies (Laurier and Mason, 2007; Liu et al., 2007; Engle et al., 2008;
375 Cheng et al., 2014). This is due to the fact that the oxidation of GEM in the MBL must be
376 photochemical, which have been evidenced by the diurnal cycle of RGM (Laurier and Mason,
377 2007). Another reason is that there was more Br (gas phase) production during daytime (Sander et
378 al., 2003). Figure S3 showed that the RGM concentration in the nighttime was lower than those in
379 corresponding forenoon and afternoon except the measurements in the PRE. This further indicated
380 that (1) the RGM originated from the photo-oxidation of Hg⁰ in the atmosphere and (2) the RGM
381 was easily and quickly removed from the atmosphere in nighttime.

382 In addition, we found that the difference in RGM concentration between day and night in the
383 SCS was higher than those in the BS and YS (Wang et al., 2016b), and one possible reason is that
384 the solar radiation and air temperature over the SCS were stronger and higher compared to those
385 over the BS and YS (Wang et al., 2016b) as a result of the specific location of the SCS (tropical
386 sea) and the different sampling time (the SCS: September 2015, the BS and YS: April–May and
387 November 2014). Secondly, it could be found that the higher the RGM concentrations in the
388 daytime, and the higher the RGM concentrations in the nighttime, but the concentrations in
389 daytime were higher than that in the corresponding nighttime throughout the sampling period (see
390 Figs. 7, S3). This is partly because the higher RH and lower air temperature in nighttime were
391 conducive to the removal of RGM (Rutter and Schauer, 2007; Amos et al., 2012). Thirdly, we
392 found that the difference in RGM concentration between different days was large though there
393 was no significantly difference in PAR values (Fig. 7). However, here again divide two kinds of



394 cases: the first kind of circumstance is that the higher RGM in the PRE (day and night)
395 presumably mainly originated from the surrounding human activities (i.e., 4–5 September 2015);
396 the second scenario is that RGM in open waters mainly originated from the in situ oxidation of
397 GEM in the MBL (Soerensen et al., 2010a; Sprovieri et al., 2010). The main reason for the large
398 difference in RGM concentration between different days was that there was large difference in
399 wind speed and RH between different days (see Fig. 2), and the discussion can be found in the
400 following paragraphs.

401 3.4.3 Daily variation of $\text{Hg}^{\text{P}}_{2.5}$

402 Figure 8 shows the $\text{Hg}^{\text{P}}_{2.5}$ concentrations in the daytime and nighttime during the entire study
403 period. The $\text{Hg}^{\text{P}}_{2.5}$ value in the daytime ($3.4 \pm 1.9 \text{ pg m}^{-3}$, $n = 20$) was slightly but not significantly
404 higher than that in the nighttime ($2.4 \pm 0.9 \text{ pg m}^{-3}$, $n = 19$) (t -test, $p > 0.1$), and this pattern was
405 consistent with the result of our previous study conducted in the open waters of YS (Wang et al.,
406 2016b). The higher $\text{Hg}^{\text{P}}_{2.5}$ concentrations in the PRE and nearshore area of the Hainan Island (Fig.
407 4 and Fig. 8) indicated that the nearshore areas were readily polluted due to the anthropogenic Hg
408 emissions, while the lower $\text{Hg}^{\text{P}}_{2.5}$ level in the open sea further suggested that the open areas of the
409 SCS suffered less anthropogenic Hg^{P} . Therefore, we postulate that the $\text{Hg}^{\text{P}}_{2.5}$ over the open SCS
410 mainly originated from the in situ formation. During the cruise in the western SCS (16–28
411 September 2015), we found elevated $\text{Hg}^{\text{P}}_{2.5}$ concentrations when the RGM concentrations were
412 high at lower wind speed (e.g., 20–22 September 2015, it was sunny all these days) (see Figs. 2, 7,
413 8). This is probably due to the transferring of RGM from the gas to the particle phase. In contrast,
414 we found that the $\text{Hg}^{\text{P}}_{2.5}$ concentrations were elevated when the RGM concentrations were low at
415 higher wind speed (e.g., 25–27 September 2015, it was cloudy these days, and there was a
416 transitory drizzly on 26 September 2015) (see Figs. 2, 7, 8). On the one hand, high wind speed
417 may increase the levels of halogen atoms (Br and Cl etc.) and sea salt aerosols in the marine
418 atmosphere, which in turn were favorable to the production of RGM and formation of $\text{Hg}^{\text{P}}_{2.5}$
419 (Auzmendi-Murua et al., 2014); on the other hand, high wind speed was favorable to the removal
420 of RGM and $\text{Hg}^{\text{P}}_{2.5}$ in the atmosphere, this was probably the reason for lower RGM and $\text{Hg}^{\text{P}}_{2.5}$
421 concentrations during 25–27 September as compared to those observed during 20–22 September
422 (see Fig. 2).

423 Pearson's correlation coefficients were calculated between speciated Hg and meteorological
424 parameters to identify the relationships between them (Table 2). According to the correlation
425 analysis, the $\text{Hg}^{\text{P}}_{2.5}$ was significantly positively correlated with RGM. Part of the reason was that
426 RGM could be adsorbed by particulate matter under high RGM concentrations and then enhanced
427 the Hg^{P} concentrations. Similarly, the $\text{Hg}^{\text{P}}_{2.5}$ had a significantly positive correlation with GEM, on
428 the one hand, GEM and Hg^{P} probably originated from the anthropogenic sources especially in the
429 PRE and nearshore areas; on the other hand, it was probably due to the fact that GEM could be



430 oxidized to form RGM and then Hg^{P} , which might be the reason for the positive but not
431 significant correlation between RGM and GEM since higher GEM level may result in higher
432 RGM level in daytime. The correlation analysis showed that the $\text{Hg}^{\text{P}_{2.5}}$ and RGM were all
433 negatively correlated with wind speed and RH (Table 2), and the higher wind speed was favorable
434 to the removal of $\text{Hg}^{\text{P}_{2.5}}$ over the RGM. This is because the high wind speed might increase the
435 RH levels and then elevated wind speed and RH may accelerate the removal of $\text{Hg}^{\text{P}_{2.5}}$ and RGM
436 (Cheng et al., 2014; Wang et al., 2016b). Moreover, both the air temperature and PAR were
437 positively correlated with RGM and $\text{Hg}^{\text{P}_{2.5}}$, and a significantly positive correlation was found
438 between PAR and RGM, indicating that the role of solar radiation played on the production of
439 RGM was more obvious than that on the formation of $\text{Hg}^{\text{P}_{2.5}}$, which were consistent with the
440 previous study at coastal and marine sites (Mao et al., 2012).

441 3.5 Sea-air exchange of Hg^0 in the SCS

442 The spatial distributions of DGM and Hg^0 fluxes in the SCS are illustrated in Fig. 9. The DGM
443 level in nearshore area was higher than that in the open sea, and this pattern was similar to our
444 previous study conducted in the ECS (Wang et al., 2016c). The DGM concentration in this study
445 varied from 23.0 to 66.8 pg l^{-1} with a mean value of $37.1 \pm 9.0 \text{ pg l}^{-1}$ (Fig. 9a and Table S3),
446 which was higher than those in other open oceans, such as the Atlantic Ocean (Anderson et al.,
447 2011), the West Atlantic Ocean and the South Pacific Ocean (Soerensen et al., 2013, 2014), but
448 considerably lower than that in the Minamata Bay (Marumoto et al., 2015). The mean DGM
449 concentration in the northern SCS ($41.3 \pm 10.9 \text{ pg l}^{-1}$) was significantly higher than that in the
450 western SCS ($33.5 \pm 5.0 \text{ pg l}^{-1}$) (*t*-test, $p < 0.01$). The reason was that DGM concentrations in the
451 nearshore areas of the PRE and Hainan Island were higher than those in the western open sea (see
452 Fig. 9a). The DGM in surface seawater of the SCS was supersaturated with a saturation of 501 %
453 to 1468 % with a mean value of $903 \pm 208 \%$, which was approximately two thirds of that
454 measured in the ECS (Wang et al., 2016c). The result indicated that (1) the surface seawater in the
455 SCS was supersaturated with gaseous Hg and (2) Hg^0 evaporated from the surface seawater to the
456 atmosphere during our study period.

457 The sea-air exchange fluxes of Hg^0 at each station are presented in Table S3, including GEM,
458 DGM, PAR, surface seawater temperature, wind speed and saturation of Hg^0 . Sea-air exchange
459 fluxes of Hg^0 in the SCS ranged from 0.40 to 12.71 $\text{ng m}^{-2} \text{ h}^{-1}$ with a mean value of 4.99 ± 3.32
460 $\text{ng m}^{-2} \text{ h}^{-1}$ (Fig. 9b and Table S3), and which was comparable to the previous measurements
461 obtained in the Mediterranean Sea, the northern SCS and the West Atlantic Ocean (Andersson et
462 al., 2007; Fu et al., 2010; Soerensen et al., 2013), but lower than those in polluted marine
463 environments, such as the Minamata Bay, the Tokyo Bay and the YS (Narukawa et al., 2006; Ci et
464 al., 2011; Marumoto et al., 2015), while higher than those in some open sea environments, such as
465 the Baltic Sea, the Atlantic Ocean and the South Pacific Ocean (Kuss and Schneider, 2007;



466 Andersson et al., 2011; Kuss et al., 2011; Soerensen et al., 2014). Interestingly, we found the Hg⁰
467 flux near the station 99 were higher than those in open water as a result of higher wind speed
468 (Table S3). In order to better understand the important role of the SCS, we relate the Hg⁰ flux in
469 the SCS to the global estimation, an annual sea-air flux of Hg⁰ was calculated based on the
470 assumption that there was no seasonal variation in Hg⁰ emission flux from the SCS. The annual
471 emission flux of Hg⁰ from the SCS was estimated to be 159.6 tons yr⁻¹ assuming the area of the
472 SCS was 3.56 × 10¹² m² (accounting for about 1.0 % of the global ocean area), which constituted
473 about 5.5 % of the global Hg⁰ oceanic evasion (Strode et al., 2007; Soerensen et al., 2010b; UNEP,
474 2013). We attributed the higher Hg⁰ flux in the SCS to the specific location of the SCS (tropical
475 sea) and the higher DGM concentrations in the SCS (especially in the northern area). Therefore,
476 the SCS may actually play an important role in the global Hg oceanic cycle. Additionally, we
477 found that the percentage of the annual dry deposition flux of atmospheric reactive Hg to the
478 annual evasion flux of Hg⁰ was approximately 18–34 %, indicating that the dry deposition of
479 atmospheric reactive Hg was an important pathway for the atmospheric Hg to the ocean.

480 **4 Conclusions**

481 During the cruise aboard the R/V *Shiyan 3* in September 2015, GEM, RGM and Hg^P were
482 determined in the MBL of the SCS. The GEM level in the SCS was comparable to the background
483 level over the global oceans due to the air masses dominantly originated from seas and oceans.
484 GEM concentrations were closely related to the sources and movement patterns of air masses
485 during this cruise. Moreover, the speciated atmospheric Hg level in the PRE was significantly
486 higher than those in the open SCS due to the anthropogenic emissions. The Hg^P concentrations in
487 coarse particles were significantly higher than those in fine particles, and the coarse modal was the
488 dominant size though there were two peaks for the size distribution of Hg^P in PM₁₀, indicating that
489 most of the Hg^P₁₀ originated from in situ production. There was no significant difference in GEM
490 and Hg^P_{2.5} concentrations between day and night, but RGM concentrations were significantly
491 higher in daytime than in nighttime. RGM was positively correlated with PAR and air temperature,
492 but negatively correlated with wind speed and RH. The DGM concentrations in nearshore areas of
493 the SCS were higher than those in the open sea, and the surface seawater of the SCS was
494 supersaturated with respect to Hg⁰. The annual flux of Hg⁰ from the SCS accounted for about
495 5.5 % of the global Hg⁰ oceanic evasion though the area of the SCS just represents 1.0 % of the
496 global ocean area, suggesting that the SCS plays an important role in the global Hg cycle.
497 Additionally, the dry deposition of atmospheric reactive Hg was a momentous pathway for the
498 atmospheric Hg to the ocean because it happens all the time.

499

500 **5 Appendix A**



501 **Table A1** List of acronyms and symbols

Abbreviation	Full name
BS	Bohai Sea
YS	Yellow Sea
ECS	East China Sea
SCS	South China Sea
PRE	Pearl River Estuary
MBL	Marine boundary layer
GEM	Gaseous elemental mercury
RGM	Reactive gaseous mercury
TAM	Total atmospheric mercury
Hg ^P _{2.1}	Particulate mercury in PM _{2.1}
Hg ^P _{2.5}	Particulate mercury in PM _{2.5}
Hg ^P ₁₀	Particulate mercury in PM ₁₀
DGM	Dissolved gaseous mercury

502

503 Data are available from the first author Chunjie Wang (888wangchunjie888@163.com).

504 *Author contributions.* XZ and ZW designed the study. CW and FH organized the mercury
505 measurements. CW performed the data analysis, and wrote the paper. All authors contributed to
506 the manuscript with discussions and comments.

507 *Competing interests.* The authors declare that they have no conflict of interest.

508 *Acknowledgments.* This research was funded by the National Basic Research Program of China
509 (No. 2013CB430002), National Natural Science Foundation of China (No. 41176066) and
510 “Strategic Priority Research Program” of the Chinese Academy of Sciences, Grant No.
511 XDB14020205. We gratefully acknowledge the open cruise organized by the South China Sea
512 Institute of Oceanology, Chinese Academy of Sciences. The technical assistance of the staff of the
513 R/V *Shiyan 3* is gratefully acknowledged.

514 **References**

- 515 Ahn, M. C., Kim, B., Holsen, T. M., Yi, S. M., and Han, Y. J.: Factors influencing concentrations of dissolved
516 gaseous mercury (DGM) and total mercury (TM) in an artificial reservoir, *Environ. Pollut.*, 158, 347–355,
517 <https://doi.org/10.1016/j.envpol.2009.08.036>, 2010.
- 518 Amos, H. M., Jacob, D. J., Holmes, C. D., Fisher, J. A., Wang, Q., Yantosca, R. M., Corbitt, E. S., Galarnau, E.,
519 Rutter, A. P., Gustin, M. S., Steffen, A., Schauer, J. J., Graydon, J. A., St. Louis, V. L., Talbot, R. W., Edgerton, E.
520 S., Zhang, Y., and Sunderland, E. M.: Gas-particle partitioning of atmospheric Hg(II) and its effect on global



- 521 mercury deposition, *Atmos. Chem. Phys.*, 12, 591–603, <https://doi.org/10.5194/acp-12-591-2012>, 2012.
- 522 Andersson, M. E., Gårdfeldt, K., Wängberg, I., Sprovieri, F., Pirrone, N., and Lindqvist, O.: Seasonal and daily
523 variation of mercury evasion at coastal and off shore sites from the Mediterranean Sea, *Mar. Chem.*, 104,
524 214–226, <https://doi.org/10.1016/j.marchem.2006.11.003>, 2007.
- 525 Andersson, M. E., Sommar, J., Gårdfeldt, K., and Jutterström, S.: Air–sea exchange of volatile mercury in the
526 North Atlantic Ocean, *Mar. Chem.*, 125, 1–7, <https://doi.org/10.1016/j.marchem.2011.01.005>, 2011.
- 527 Angot, H., Barret, M., Magand, O., Ramonet, M., Dommergue, A.: A 2-year record of atmospheric mercury
528 species at a background Southern Hemisphere station on Amsterdam Island, *Atmos. Chem. Phys.*, 14,
529 11461–11473, <https://doi.org/10.5194/acp-14-11461-2014>, 2014
- 530 Ariya, P. A., Amyot, M., Dastoor, A., Deeds, D., Feinberg, A., Kos, G., Poulain, A., Ryjkov, A., Semeniuk, K.,
531 Subir, M., and Toyota, K.: Mercury Physicochemical and Biogeochemical Transformation in the Atmosphere
532 and at Atmospheric Interfaces: A Review and Future Directions, *Chem. Rev.*, 115, 3760–3802,
533 <https://doi.org/10.1021/cr500667e>, 2015.
- 534 Athanassopoulou, E., Tombrou, M., Pandis, S. N., and Russell, A. G.: The role of sea-salt emissions and
535 heterogeneous chemistry in the air quality of polluted coastal areas, *Atmos. Chem. Phys.*, 8, 5755–5769,
536 <https://doi.org/10.5194/acp-8-5755-2008>, 2008.
- 537 Auzmendi-Murua, I., Castillo, Á., and Bozzelli, J. W.: Mercury oxidation via chlorine, bromine, and iodine under
538 atmospheric conditions: Thermochemistry and kinetics, *J. Phys. Chem. A*, 118, 2959–2975,
539 <https://doi.org/10.1021/jp412654s>, 2014.
- 540 Bowman, K. L., Hammerschmidt, C. R., Lamborg, C. H., and Swarr, G.: Mercury in the North Atlantic Ocean: the
541 U.S. Geotraces zonal and Meridional sections, *Deep Sea Res. Part II*, 116, 251–261,
542 <https://doi.org/10.1016/j.dsr2.2014.07.004>, 2015.
- 543 Chand, D., Jaffe, D., Prestbo, E., Swartzendruber, P. C., Hafner, W., Weiss-Penzias, P., Kato, S., Takami, A.,
544 Hatakeyama, S., and Kajii, Y.: Reactive and particulate mercury in the Asian marine boundary layer, *Atmos.*
545 *Environ.*, 42, 7988–7996, <https://doi.org/10.1016/j.atmosenv.2008.06.048>, 2008.
- 546 Cheng, I., Zhang, L., Blanchard, P., Graydon, J. A., and St. Louis, V. L.: Source-receptor relationships for speciated
547 atmospheric mercury at the remote Experimental Lakes Area, northwestern Ontario, Canada, *Atmos. Chem.*
548 *Phys.*, 12, 1903–1922, <https://doi.org/10.5194/acp-12-1903-2012>, 2012.
- 549 Cheng, I., Zhang, L., Blanchard, P., Dalziel, J., Tordon, R., Huang, J., and Holsen, T. M.: Comparisons of mercury
550 sources and atmospheric mercury processes between a coastal and inland site, *J. Geophys. Res.*, 118, 2434–2443,
551 <https://doi.org/10.1002/jgrd.50169>, 2013.
- 552 Cheng, I., Zhang, L., Mao, H., Blanchard, P., Tordon, R., and Dalziel, J.: Seasonal and diurnal patterns of speciated
553 atmospheric mercury at a coastal-rural and a coastal-urban site, *Atmos. Environ.*, 82, 193–205,
554 <https://doi.org/10.1016/j.atmosenv.2013.10.016>, 2014.
- 555 Choi, H. D., Holsen, T. M., and Hopke, P. K.: Atmospheric mercury (Hg) in the Adirondacks: Concentrations and
556 sources, *Environ. Sci. Technol.*, 42, 5644–5653, <https://doi.org/10.1021/es7028137>, 2008.
- 557 Ci, Z., Zhang, X., Wang, Z., Niu, Z., Diao, X., and Wang, S.: Distribution and air–sea exchange of mercury (Hg) in



- 558 the Yellow Sea, *Atmos. Chem. Phys.*, 11, 2881–2892, <https://doi.org/10.5194/acp-11-2881-2011>, 2011.
- 559 Ci, Z., Wang, C., Wang, Z., and Zhang, X.: Elemental mercury (Hg(0)) in air and surface waters of the Yellow Sea
560 during late spring and late fall 2012: Concentration, spatial-temporal distribution and air/sea flux, *Chemosphere*,
561 119, 199–208, <https://doi.org/10.1016/j.chemosphere.2014.05.064>, 2015.
- 562 de Foy, B., Tong, Y., Yin, X., Zhang, W., Kang, S., Zhang, Q., Zhang, G., Wang, X., Schauer, J. J.: First field-based
563 atmospheric observation of the reduction of reactive mercury driven by sunlight, *Atmos. Environ.*, 134, 27–39,
564 <https://doi.org/10.1016/j.atmosenv.2016.03.028>, 2016.
- 565 Draxler, R. R., and Rolph, G. D.: HYSPLITModel access via NOAA ARL READY Website
566 (<http://www.arl.noaa.gov/ready/hysplit4.html>), NOAA Air Resources Laboratory, Silver Spring, MD, 2012.
- 567 Engle, M. A., Tate, M. T., Krabbenhoft, D. P., Kolker, A., Olson, M. L., Edgerton, E. S., DeWild, J. F., and
568 McPherson, A. K.: Characterization and cycling of atmospheric mercury along the central US Gulf Coast, *Appl.*
569 *Geochem.*, 23, 419–437, <https://doi.org/10.1016/j.apgeochem.2007.12.024>, 2008.
- 570 Feddersen, D. M., Talbot, R., Mao, H., and Sive, B. C.: Size distribution of particulate mercury in marine and
571 coastal atmospheres, *Atmos. Chem. Phys.*, 12, 10899–10909, <https://doi.org/10.5194/acp-12-10899-2012>, 2012.
- 572 Fitzgerald, W. F., Lamborg, C. H., and Hammerschmidt, C. R.: Marine biogeochemical cycling of mercury, *Chem.*
573 *Rev.*, 107, 641–662, <https://doi.org/10.1021/cr050353m>, 2007.
- 574 Fu, X., Feng, X., Zhang, G., Xu, W., Li, X., Yao, H., Liang, P., Li, J., Sommar, J., Yin, R., and Liu, N.: Mercury in
575 the marine boundary layer and seawater of the South China Sea: Concentrations, sea/air flux, and implication for
576 land outflow, *J. Geophys. Res.*, 115, D06303, <https://doi.org/10.1029/2009JD012958>, 2010.
- 577 Fu, X., Feng, X., Qiu, G., Shang, L., and Zhang, H.: Speciated atmospheric mercury and its potential source in
578 Guiyang, China, *Atmos. Environ.*, 45, 4205–4212, <https://doi.org/10.1016/j.atmosenv.2011.05.012>, 2011.
- 579 Fu, X., Feng, X., Liang, P., Deliger, Zhang, H., Ji, J., and Liu, P.: Temporal trend and sources of speciated
580 atmospheric mercury at Waliguan GAW station, Northwestern China, *Atmos. Chem. Phys.*, 12, 1951–1964,
581 <https://doi.org/10.5194/acp-12-1951-2012>, 2012.
- 582 Gratz, L. E., Ambrose, J. L., Jaffe, D. A., Shah, V., Jaegle, L., Stutz, J., Festa, J., Spolaor, M., Tsai, C., Selin, N. E.,
583 Song, S., Zhou, X., Weinheimer, A. J., Knapp, D. J., Montzka, D. D., Flocke, F. M., Campos, T. L., Apel, E.,
584 Hornbrook, R., Blake, N. J., Hall, S., Tyndall, G. S., Reeves, M., Stechman, D., and Stell, M.: Oxidation of
585 mercury by bromine in the subtropical Pacific free troposphere, *Geophys. Res. Lett.*, 42, 10494–10502,
586 <https://doi.org/10.1002/2015GL066645>, 2015.
- 587 Giorgi, F.: Dry deposition velocities of atmospheric aerosols as inferred by applying a particle dry deposition
588 parameterisation to a general circulation model, *Tellus*, 40B, 23–41,
589 <https://doi.org/10.1111/j.1600-0889.1988.tb00210.x>, 1988.
- 590 Gustin, M. S., Huang, J., Miller, M. B., Peterson, C., Jaffe, D. A., Ambrose, J., Finley, B. D., Lyman, S. N., Call,
591 K., Talbot, R., Feddersen, D., Mao, H., and Lindberg, S. E.: Do we understand what the mercury speciation
592 instruments are actually measuring? Results of RAMIX, *Environ. Sci. Technol.*, 47, 7295–7306,
593 <https://doi.org/10.1021/es3039104>, 2013.
- 594 Hammerschmidt, C. R., and Bowman, K. L.: Vertical methylmercury distribution in the subtropical North Pacific



- 595 Ocean, *Mar. Chem.*, 132–133, 77–82, <https://doi.org/10.1016/j.marchem.2012.02.005>, 2012.
- 596 Hedgecock, I. and Pirrone, N.: Mercury and photochemistry in the marine boundary layer-modelling studies
597 suggest the in situ production of reactive gas phase mercury, *Atmos. Environ.*, 35, 3055–3062,
598 [https://doi.org/10.1016/S1352-2310\(01\)00109-1](https://doi.org/10.1016/S1352-2310(01)00109-1), 2001.
- 599 Hedgecock, I. M., Pirrone, N., Sprovieri, F., and Pesenti, E.: Reactive gaseous mercury in the marine boundary
600 layer: modeling and experimental evidence of its formation in the Mediterranean region, *Atmos. Environ.*, 37,
601 S41–S49, [https://doi.org/10.1016/S1352-2310\(03\)00236-X](https://doi.org/10.1016/S1352-2310(03)00236-X), 2003.
- 602 Holmes, C. D., Jacob, D. J., and Yang, X.: Global lifetime of elemental mercury against oxidation by atomic
603 bromine in the free troposphere, *Geophys. Res. Lett.*, 33, L20808, <https://doi.org/10.1029/2006gl027176>, 2006.
- 604 Holmes, C. D., Jacob, D. J., Mason, R. P., and Jaffe, D. A.: Sources and deposition of reactive gaseous mercury in
605 the marine atmosphere, *Atmos. Environ.*, 43, 2278–2285, <https://doi.org/10.1016/j.atmosenv.2009.01.051>, 2009.
- 606 Holmes, C. D., Jacob, D. J., Corbitt, E. S., Mao, J., Yang, X., Talbot, R., and Slemr, F.: Global atmospheric model
607 for mercury including oxidation by bromine atoms, *Atmos. Chem. Phys.*, 10, 12037–12057,
608 <https://doi.org/10.5194/acp-10-12037-2010>, 2010.
- 609 Horowitz, H. M., Jacob, D. J., Zhang, Y., Dibble, T. S., Slemr, F., Amos, H. M., Schmidt, J. A., Corbitt, E. S.,
610 Marais, E. A., and Sunderland, E. M.: A new mechanism for atmospheric mercury redox chemistry: implications
611 for the global mercury budget, *Atmos. Chem. Phys.*, 17, 6353–6371, <https://doi.org/10.5194/acp-17-6353-2017>,
612 2017.
- 613 Horvat, M., Kotnik, J., Logar, M., Fajon, V., Zvonarić, T., and Pirrone, N.: Speciation of mercury in surface and
614 deep-sea waters in the Mediterranean Sea, *Atmos. Environ.*, 37, S93–S108,
615 [https://doi.org/10.1016/S1352-2310\(03\)00249-8](https://doi.org/10.1016/S1352-2310(03)00249-8), 2003.
- 616 Howard, D., Nelson, P. F., Edwards, G. C., Morrison, A. L., Fisher, J. A., Ward, J., Harnwell, J., van der Schoot, M.,
617 Atkinson, B., Chambers, S. D., Griffiths, A. D., Werczynski, S., and Williams, A. G.: Atmospheric mercury in
618 the Southern Hemisphere tropics: seasonal and diurnal variations and influence of inter-hemispheric transport,
619 *Atmos. Chem. Phys.*, 17, 11623–11636, <https://doi.org/10.5194/acp-17-11623-2017>, 2017.
- 620 Huang, J., Miller, M. B., Edgerton, E., and Sexauer Gustin, M.: Deciphering potential chemical compounds of
621 gaseous oxidized mercury in Florida, USA, *Atmos. Chem. Phys.*, 17, 1689–1698,
622 <https://doi.org/10.5194/acp-17-1689-2017>, 2017.
- 623 Kim, S. H., Han, Y. J., Holsen, T. M., and Yi, S. M.: Characteristics of atmospheric speciated mercury
624 concentrations (TGM, Hg(II) and Hg(p)) in Seoul, Korea, *Atmos. Environ.*, 43, 3267–3274,
625 <https://doi.org/10.1016/j.atmosenv.2009.02.038>, 2009.
- 626 Kim, P. R., Han, Y. J., Holsen, T. M., and Yi, S. M.: Atmospheric particulate mercury: Concentrations and size
627 distributions, *Atmos. Environ.*, 61, 94–102, <https://doi.org/10.1016/j.atmosenv.2012.07.014>, 2012.
- 628 Kuss, J.: Water–air gas exchange of elemental mercury: An experimentally determined mercury diffusion
629 coefficient for Hg⁰ water–air flux calculations, *Limnol. Oceanogr.*, 59, 1461–1467,
630 <https://doi.org/10.4319/lo.2014.59.5.1461>, 2014.
- 631 Kuss, J., and Schneider, B.: Variability of the gaseous elemental mercury sea-air flux of the Baltic Sea, *Environ.*



- 632 Sci. Technol., 41, 8018–8023, <https://doi.org/10.1021/es0716251>, 2007.
- 633 Kuss, J., Züticke, C., Pohl, C., and Schneider, B.: Atlantic mercury emission determined from continuous analysis
634 of the elemental mercury sea-air concentration difference within transects between 50°N and 50°S, *Global*
635 *Biogeochem. Cycles*, 25, GB 3021, <https://doi.org/10.1029/2010GB003998>, 2011.
- 636 Kuss, J., Krüger, S., Ruickoldt, J., and Wlost, K.-P.: High-resolution measurements of elemental mercury in
637 surface water for an improved quantitative understanding of the Baltic Sea as a source of atmospheric mercury,
638 *Atmos. Chem. Phys.*, 18, 4361–4376, <https://doi.org/10.5194/acp-18-4361-2018>, 2018.
- 639 Landis, M. S., Stevens, R. K., Schaedlich, F., and Prestbo, E. M.: Development and characterization of an annular
640 denuder methodology for the measurement of divalent inorganic reactive gaseous mercury in ambient air,
641 *Environ. Sci. Technol.*, 36, 3000–3009, <https://doi.org/10.1021/es015887t>, 2002.
- 642 Laurier, F. J. G., Mason, R. P., Whalin, L., and Kato, S.: Reactive gaseous mercury formation in the North Pacific
643 Ocean's marine boundary layer: A potential role of halogen chemistry, *J. Geophys. Res.*, 108, 4529,
644 <https://doi.org/10.1029/2003JD003625>, 2003.
- 645 Laurier, F., and Mason, R.: Mercury concentration and speciation in the coastal and open ocean boundary layer, *J.*
646 *Geophys. Res.*, 112, D06302, <https://doi.org/10.1029/2006JD007320>, 2007.
- 647 Lindberg, S. E., and Stratton, W. J.: Atmospheric mercury speciation: Concentrations and behavior of reactive
648 gaseous mercury in ambient air, *Environ. Sci. Technol.*, 32, 49–57, <https://doi.org/10.1021/es970546u>, 1998.
- 649 Lindberg, S. E., Brooks, S., Lin, C. J., Scott, K. J., Landis, M. S., Stevens, R. K., Goodsite, M., and Richter, A.:
650 Dynamic oxidation of gaseous mercury in the Arctic troposphere at polar sunrise, *Environ. Sci. Technol.*, 36,
651 1245–1256, <https://doi.org/10.1021/es0111941>, 2002.
- 652 Liss, P. W., and Slater, P. G.: Flux of gases across the air-sea interface, *Nature*, 247, 181–184,
653 <https://doi.org/10.1038/247181a0>, 1974.
- 654 Liu, B., Keeler, G. J., Dvonch, J. T., Barres, J. A., Lynam, M. M., Marsik, F. J., and Morgan, J. T.: Temporal
655 variability of mercury speciation in urban air, *Atmos. Environ.*, 41, 1911–1923,
656 <https://doi.org/10.1016/j.atmosenv.2006.10.063>, 2007.
- 657 Liu, B., Keeler, G. J., Dvonch, J. T., Barres, J. A., Lynam, M. M., Marsik, F. J., and Morgan, J. T.: Urban-rural
658 differences in atmospheric mercury speciation, *Atmos. Environ.*, 44, 2013–2023,
659 <https://doi.org/10.1016/j.atmosenv.2010.02.012>, 2010.
- 660 Liu, N., Qiu, G., Landis, M., Feng, X., Fu, X., and Shang, L.: Atmospheric mercury species measured in Guiyang,
661 Guizhou province, southwest China, *Atmos. Res.*, 100, 93–102, <https://doi.org/10.1016/j.atmosres.2011.01.002>,
662 2011.
- 663 Mamane, Y., Perrino, C., Yossef, O., and Catrambone, M.: Source characterization of fine and coarse particles at
664 the East mediterranean coast, *Atmos. Environ.*, 42, 6114–6130, doi:10.1016/j.atmosenv.2008.02.045, 2008.
- 665 Mao, H., Talbot, R., Hegarty, J., and Koerner, J.: Speciated mercury at marine, coastal, and inland sites in New
666 England – Part 2: Relationships with atmospheric physical parameters, *Atmos. Chem. Phys.*, 12, 4181–4206,
667 <https://doi.org/10.5194/acp-12-4181-2012>, 2012.
- 668 Mao, H., Cheng, I., and Zhang, L.: Current understanding of the driving mechanisms for spatiotemporal variations



- 669 of atmospheric speciated mercury: a review, *Atmos. Chem. Phys.*, 16, 12897-12924,
670 <https://doi.org/10.5194/acp-16-12897-2016>, 2016.
- 671 Marumoto, K., and Imai, S.: Determination of dissolved gaseous mercury in seawater of Minamata Bay and
672 estimation for mercury exchange across air-sea interface, *Mar. Chem.*, 168, 9–17,
673 <https://doi.org/10.1016/j.marchem.2014.09.007>, 2015.
- 674 Mason, R. P., Rolffhus, K. R., and Fitzgerald, W. F.: Methylated and elemental mercury cycling in surface and deep
675 ocean waters of the north Atlantic, *Water Air Soil Pollut.*, 80, 665–677, doi:10.1007/BF01189719, 1995.
- 676 Mason, R. P., and Sheu, G. R.: Role of the ocean in the global mercury cycle, *Global Biogeochem. Cycles*, 16,
677 1093, <https://doi.org/10.1029/2001GB001440>, 2002.
- 678 Mason, R. P., Choi, A. L., Fitzgerald, W. F., Hammerschmidt, C. R., Lamborg, C. H., Soerensen, A. L., and
679 Sunderland, E. M.: Mercury biogeochemical cycling in the ocean and policy implications, *Environ. Res.*, 119,
680 101–117, doi:10.1016/j.envres.2012.03.013, 2012.
- 681 Mason, R. P., Hammerschmidt, C. R., Lamborg, C. H., Bowman, K. L., Swarr, G. J., and Shelley, R. U.: The air-sea
682 exchange of mercury in the low latitude Pacific and Atlantic Oceans, *Deep Sea Res. Part I*, 122, 17–28,
683 <https://doi.org/10.1016/j.dsr.2017.01.015>, 2017.
- 684 Narukawa, M., Sakata, M., Marumoto, K., and Asakura, K.: Air-sea exchange of mercury in Tokyo Bay, *J.*
685 *Oceanogr.*, 62, 249–257, <https://doi.org/10.1007/s10872-006-0049-3>, 2006.
- 686 Nho-Kim, E. Y., Michou, M., and Peuch, V. H.: Parameterization of size-dependent particle dry deposition
687 velocities for global modeling, *Atmos. Environ.*, 38, 1933–1942, <https://doi.org/10.1016/j.atmosenv.2004.01.002>,
688 2004.
- 689 Poissant, L., Pilote, M., Xu, X., Zhang, H. and Beauvais C.: Atmospheric mercury speciation and deposition in the
690 Bay St. François wetlands, *J. Geophys. Res.*, 109, D11301, <https://doi.org/10.1029/2003JD004364>, 2004.
- 691 Pryor, S. C., and Sorensen, L. L.: Nitric acid-sea salt reactions: Implications for nitrogen deposition to water
692 surfaces, *J. Appl. Meteorol.*, 39, 725–731, <https://doi.org/10.1175/1520-0450-39.5.725>, 2000.
- 693 Radke, L. F., Friedli, H. R., and Heikes, B. G.: Atmospheric mercury over the NE Pacific during spring 2002:
694 Gradients, residence time, upper troposphere lower stratosphere loss, and long-range transport, *J. Geophys. Res.*,
695 112, D19305, <https://doi.org/10.1029/2005JD005828>, 2007.
- 696 Read, K. A., Neves, L. M., Carpenter, L. J., Lewis, A. C., Fleming, Z. L., and Kentisbeer, J.: Four years
697 (2011–2015) of total gaseous mercury measurements from the Cape Verde Atmospheric Observatory, *Atmos.*
698 *Chem. Phys.*, 17, 5393-5406, <https://doi.org/10.5194/acp-17-5393-2017>, 2017.
- 699 Rutter, A. P., and Schauer, J. J.: The effect of temperature on the gas-particle partitioning of reactive mercury in
700 atmospheric aerosols, *Atmos. Environ.*, 41, 8647–8657, <https://doi.org/10.1016/j.atmosenv.2007.07.024>, 2007.
- 701 Sander, R., Keene, W. C., Pszenny, A. A. P., Arimoto, R., Ayers, G. P., Baboukas, E., Cainey, J. M., Crutzen, P. J.,
702 Duce, R. A., Hönninger, G., Huebert, B. J., Maenhaut, W., Mihalopoulos, N., Turekian, V. C., and Van Dingenen,
703 R., Inorganic bromine in the marine boundary layer: a critical review, *Atmos. Chem. Phys.*, 3, 1301–1336,
704 <https://doi.org/10.5194/acp-3-1301-2003>, 2003.
- 705 Schroeder, W. H., and Munthe, J.: Atmospheric mercury – An overview, *Atmos. Environ.*, 32, 809–822,



- 706 [https://doi.org/10.1016/S1352-2310\(97\)00293-8](https://doi.org/10.1016/S1352-2310(97)00293-8), 1998.
- 707 Seigneur, C., and Lohman, K.: Effect of bromine chemistry on the atmospheric mercury cycle, *J. Geophys. Res.*,
- 708 113, D23309, <https://doi.org/10.1029/2008JD010262>, 2008.
- 709 Selin, N. E., Jacob, D. J., Park, R. J., Yantosca, R. M., Strode, S., Jaeglé L., and Jaffe, D.: Chemical cycling and
- 710 deposition of atmospheric mercury: Global constraints from observations, *J. Geophys. Res.*, 112, D02308,
- 711 <https://doi.org/10.1029/2006JD007450>, 2007.
- 712 Shah, V., Jaeglé L., Gratz, L. E., Ambrose, J. L., Jaffe, D. A., Selin, N. E., Song, S., Campos, T. L., Flocke, F. M.,
- 713 Reeves, M., Stechman, D., Stell, M., Festa, J., Stutz, J., Weinheimer, A. J., Knapp, D. J., Montzka, D. D.,
- 714 Tyndall, G. S., Apel, E. C., Hornbrook, R. S., Hills, A. J., Riemer, D. D., Blake, N. J., Cantrell, C. A., and
- 715 Mauldin III, R. L.: Origin of oxidized mercury in the summertime free troposphere over the southeastern US,
- 716 *Atmos. Chem. Phys.*, 16, 1511-1530, <https://doi.org/10.5194/acp-16-1511-2016>, 2016.
- 717 Sheu, G. R., and Mason, R. P.: An examination of the oxidation of elemental mercury in the presence of halide
- 718 surfaces, *J. Atmos. Chem.*, 48, 107-130, <https://doi.org/10.1023/B:JOCH.0000036842.37053.e6>, 2004.
- 719 Slemr, F., Angot, H., Dommergue, A., Magand, O., Barret, M., Weigelt, A., Ebinghaus, R., Brunke, E.-G.,
- 720 Pfaffhuber, K. A., Edwards, G., Howard, D., Powell, J., Keywood, M., and Wang, F.: Comparison of mercury
- 721 concentrations measured at several sites in the Southern Hemisphere, *Atmos. Chem. Phys.*, 15, 3125-3133,
- 722 <https://doi.org/10.5194/acp-15-3125-2015>, 2015.
- 723 Soerensen, A. L., Skov, H., Jacob, D. J., Soerensen, B. T., and Johnson, M. S.: Global concentrations of gaseous
- 724 elemental mercury and reactive gaseous mercury in the marine boundary layer, *Environ. Sci. Technol.*, 44,
- 725 7425-7430, <https://doi.org/10.1021/es903839n>, 2010a.
- 726 Soerensen, A. L., Sunderland, E. M., Holmes, C. D., Jacob, D. J., Yantosca, R. M., Skov, H., Christensen, J. H.,
- 727 Strode, S. A., and Mason, R. P.: An improved global model for air-sea exchange of mercury: high concentrations
- 728 over the North Atlantic, *Environ. Sci. Technol.*, 44, 8574-8580, <https://doi.org/10.1021/es102032g>, 2010b.
- 729 Soerensen, A. L., Mason, R. P., Balcom, P. H., and Sunderland, E. M.: Drivers of surface ocean mercury
- 730 concentrations and air-sea exchange in the west Atlantic Ocean, *Environ. Sci. Technol.*, 47, 7757-7765,
- 731 <https://doi.org/10.1021/es401354q>, 2013.
- 732 Soerensen, A. L., Mason, R. P., Balcom, P. H., Jacob, D. J., Zhang, Y., Kuss, J., and Sunderland, E. M.: Elemental
- 733 mercury concentrations and fluxes in the tropical atmosphere and ocean, *Environ. Sci. Technol.*, 48,
- 734 11312-11319, <https://doi.org/10.1021/es503109p>, 2014.
- 735 Sprovieri, F., Pirrone, N., Gärdfeldt, K., and Sommar, J.: Mercury speciation in the marine boundary layer along a
- 736 6000 km cruise path around the Mediterranean Sea, *Atmos. Environ.*, 37, S63-S71,
- 737 [https://doi.org/10.1016/S1352-2310\(03\)00237-1](https://doi.org/10.1016/S1352-2310(03)00237-1), 2003.
- 738 Sprovieri, F., and Pirrone, N.: Spatial and temporal distribution of atmospheric mercury species over the Adriatic
- 739 Sea, *Environ. Fluid Mech.*, 8, 117-128, <https://doi.org/10.1007/s10652-007-9045-4>, 2008.
- 740 Sprovieri, F., Hedgecock, I. M., and Pirrone, N.: An investigation of the origins of reactive gaseous mercury in the
- 741 Mediterranean marine boundary layer, *Atmos. Chem. Phys.*, 10, 3985-3997,
- 742 <https://doi.org/10.5194/acp-10-3985-2010>, 2010.



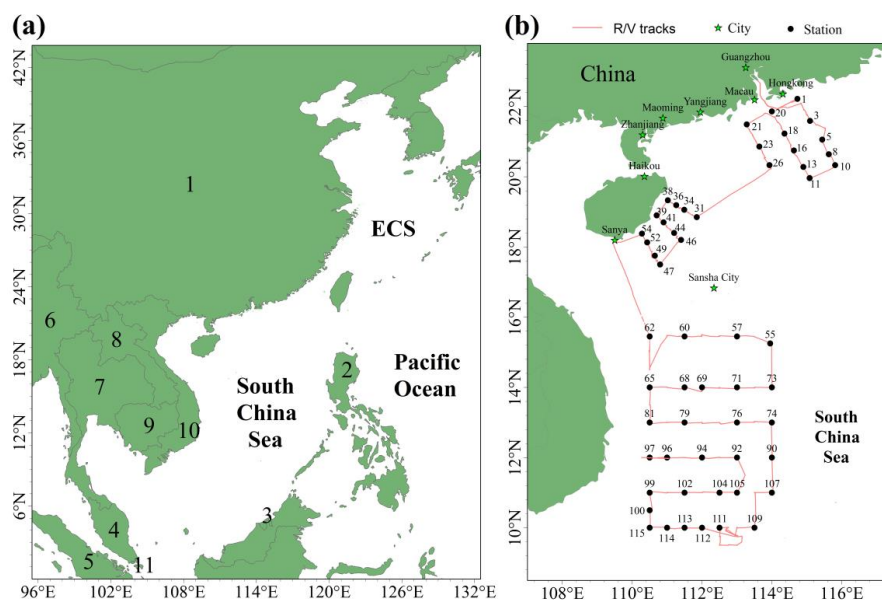
- 743 Steffen, A., Lehnherr, I., Cole, A., Ariya, P., Dastoor, A., Durnford, D., Kirk, J., and Pilote, M.: Atmospheric
744 mercury measurements in the Canadian Arctic Part I: A review of recent field measurements, *Sci. Total Environ.*,
745 509–510, 3–15, <https://doi.org/10.1016/j.scitotenv.2014.10.109>, 2015.
- 746 Strode, S. A., Jaeglé L., Selin, N. E., Jacob, D. J., Park, R. J., Yantosca, R. M., Mason, R. P., and Slemr, F.: Air-sea
747 exchange in the global mercury cycle, *Global Biogeochem. Cycles*, 21, GB1017,
748 <https://doi.org/10.1029/2006GB002766>, 2007.
- 749 Tseng, C. M., Liu, C. S., and Lamborg, C.: Seasonal changes in gaseous elemental mercury in relation to monsoon
750 cycling over the northern South China Sea, *Atmos. Chem. Phys.*, 12, 7341–7350,
751 <https://doi.org/10.5194/acp-12-7341-2012>, 2012.
- 752 UNEP: Global Mercury Assessment: Sources, Emissions, Releases and Environmental Transport, UNEP
753 Chemicals Branch, Geneva, Switzerland, 2013.
- 754 Valente, R. J., Shea, C., Humes, K. L., and Tanner, R. L.: Atmospheric mercury in the Great Smoky Mountains
755 compared to regional and global levels, *Atmos. Environ.*, 41, 1861–1873,
756 <https://doi.org/10.1016/j.atmosenv.2006.10.054>, 2007.
- 757 Wang, Y. Q., Zhang, X. Y., and Draxler, R. R.: TrajStat: GIS-based software that uses various trajectory statistical
758 analysis methods to identify potential sources from long-term air pollution measurement data, *Environ. Model.*
759 *Softw.*, 28, 938–939, <https://doi.org/10.1016/j.envsoft.2009.01.004>, 2009.
- 760 Wang, S., Schmidt, J. A., Baidar, S., Coburn, S., Dix, B., Koenig, T. K., Apel, E., Bowdalo, D., Campos, T. L.,
761 Eloranta, E., Evans, M. J., DiGangi, J. P., Zondlo, M. A., Gao, R. S., Haggerty, J. A., Hall, S. R., Hornbrook, R.
762 S., Jacob, D., Morley, B., Pierce, B., Reeves, M., Romashkin, P., ter Schure, A., and Volkamer, R.: Active and
763 widespread halogen chemistry in the tropical and subtropical free troposphere, *Proc. Natl. Acad. Sci. U.S.A.*,
764 112, 9281–9286, <https://doi.org/10.1073/pnas.1505142112>, 2015.
- 765 Wang, C., Wang, Z., Ci, Z., Zhang, X., and Tang, X.: Spatial-temporal distributions of gaseous element mercury
766 and particulate mercury in the Asian marine boundary layer, *Atmos. Environ.*, 126, 107–116,
767 <https://doi.org/10.1016/j.atmosenv.2015.11.036>, 2016a.
- 768 Wang, C., Ci, Z., Wang, Z., Zhang, X., and Guo, J.: Speciated atmospheric mercury in the marine boundary layer
769 of the Bohai Sea and Yellow Sea, *Atmos. Environ.*, 131, 360–370,
770 <https://doi.org/10.1016/j.atmosenv.2016.02.021>, 2016b.
- 771 Wang, C., Ci, Z., Wang, Z., and Zhang, X.: Air-sea exchange of gaseous mercury in the East China Sea, *Environ.*
772 *Pollut.*, 212, 535–543, <https://doi.org/10.1016/j.envpol.2016.03.016>, 2016c.
- 773 Wanninkhof, R.: Relationship between wind speed and gas exchange over the ocean, *J. Geophys. Res.*, 97,
774 7373–7382, <https://doi.org/10.1029/92JC00188>, 1992.
- 775 Weiss-Penzias, P., Jaffe, D. A., McClintick, A., Prestbo, E. M., and Landis, M. S.: Gaseous elemental mercury in
776 the marine boundary layer: Evidence for rapid removal in anthropogenic pollution, *Environ. Sci. Technol.*, 37,
777 3755–3763, <https://doi.org/10.1021/es0341081>, 2003.
- 778 Witt, M. L. I., Mather, T. A., Baker, A. R., De Hoog, J. C. M., and Pyle, D. M.: Atmospheric trace metals over the
779 south-west Indian Ocean: Total gaseous mercury, aerosol trace metal concentrations and lead isotope ratios, *Mar.*



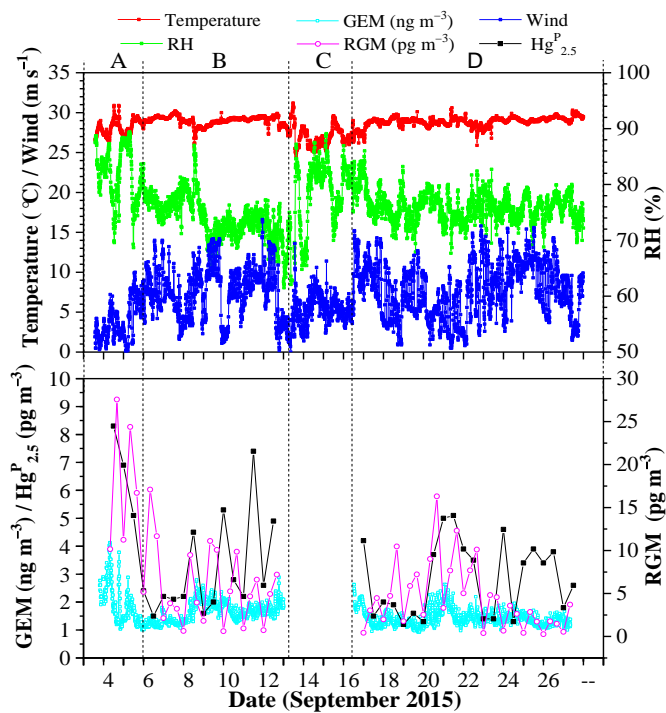
780 Chem., 121, 2–16, <https://doi.org/10.1016/j.marchem.2010.02.005>, 2010.
781 Xu, L., Chen, J., Yang, L., Niu, Z., Tong, L., Yin, L., and Chen, Y.: Characteristics and sources of atmospheric
782 mercury speciation in a coastal city, Xiamen, China, *Chemosphere*, 119, 530–539,
783 <https://doi.org/10.1016/j.chemosphere.2014.07.024>, 2015.
784 Zhu, J., Wang, T., Talbot, R., Mao, H., Yang, X., Fu, C., Sun, J., Zhuang, B., Li, S., Han, Y., and Xie, M.:
785 Characteristics of atmospheric mercury deposition and size-fractionated particulate mercury in urban Nanjing,
786 China, *Atmos. Chem. Phys.*, 14, 2233–2244, <https://doi.org/10.5194/acp-14-2233-2014>, 2014.

787

788 **Figures and Tables**



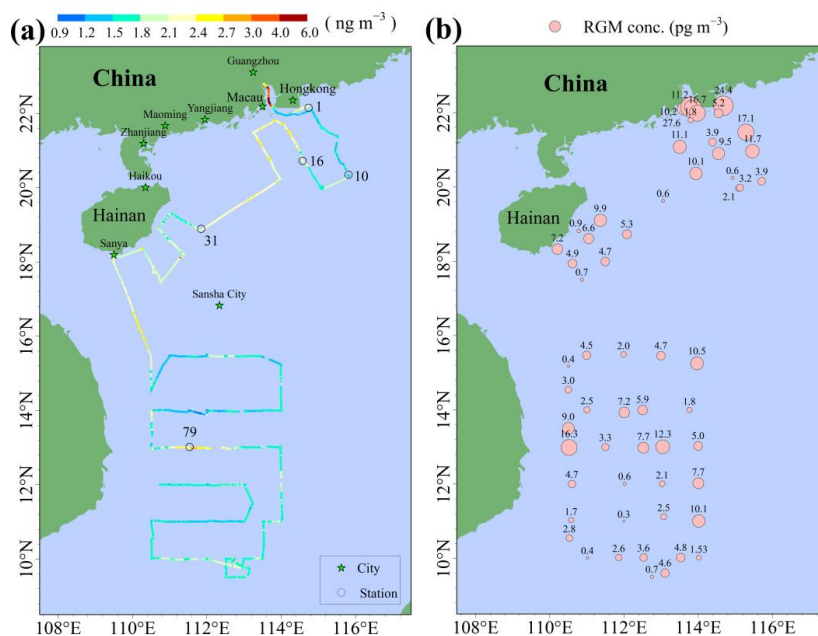
789 **Figure 1.** Map of the South China Sea (a) (1: China, 2: Philippines, 3: Brunei, 4: Malaysia, 5:
790 Indonesia, 6: Myanmar, 7: Thailand, 8: Laos, 9: Cambodia, 10: Vietnam, 11: Singapore), and
791 locations of the DGM sampling station and the R/V tracks (b). It should be noted that the black
792 solid points represent the sampling stations, and the number near the black solid point represents
793 the name of the station.
794



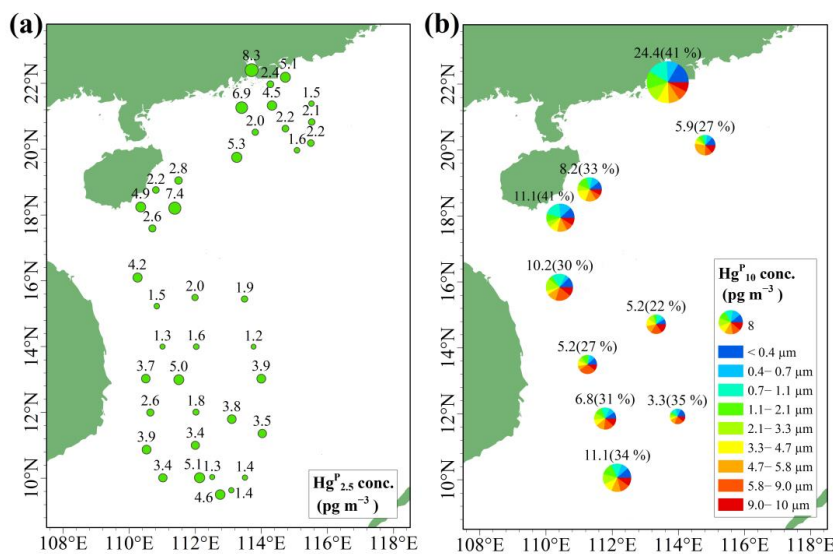
795

796 **Figure 2.** Time (local time) series of GEM, Hg^P_{2.5}, RGM and some meteorological parameters,
 797 including relative humidity (RH), air temperature and wind speed (“A” represents the data
 798 measured in the Pearl River Estuary (PRE), “B” represents the data measured in the northern SCS,
 799 “C” represents the data obtained in the port of Sanya, “D” represents the data measured in the
 800 western SCS). It was rainy day on the days of 8 and 26 September 2015.

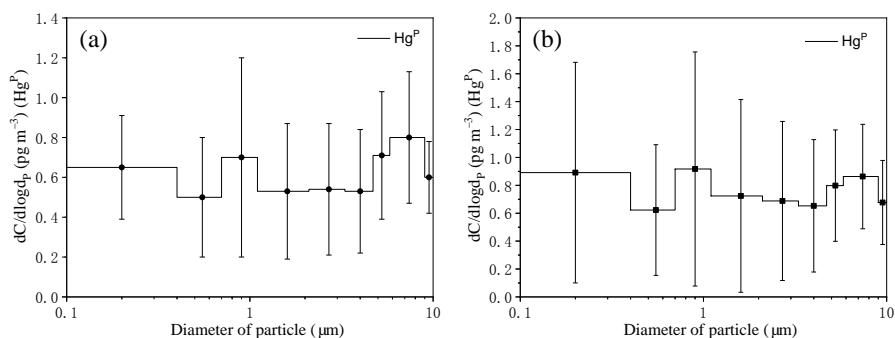
801



802
 803 **Figure 3.** The concentrations and spatial distributions of GEM (a) and RGM (b) in the MBL of the
 804 SCS.



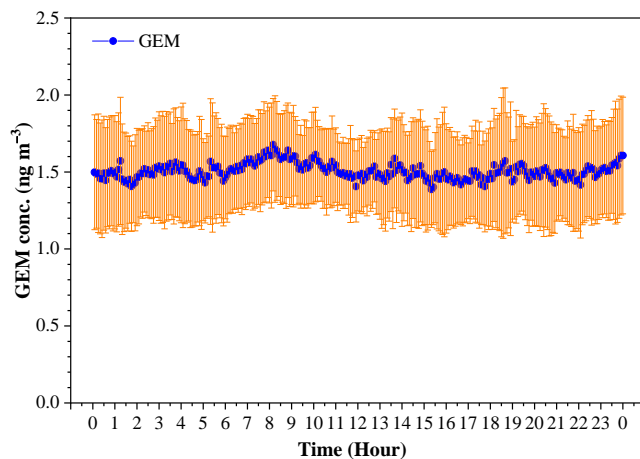
805
 806 **Figure 4.** Spatial distributions of $\text{Hg}^{\text{P}}_{2.5}$ (a) and $\text{Hg}^{\text{P}}_{10}$ ($\text{Hg}^{\text{P}}_{2.1}/\text{Hg}^{\text{P}}_{10}$ ratio) (b) in the MBL of the
 807 SCS. $\text{Hg}^{\text{P}}_{2.5}$, $\text{Hg}^{\text{P}}_{2.1}$ and $\text{Hg}^{\text{P}}_{10}$ denote the Hg^{P} in $\text{PM}_{2.5}$, $\text{PM}_{2.1}$ and PM_{10} , respectively.
 808



809

810 **Figure 5.** Size distributed concentrations of Hg^{P} (PM_{10}) in the MBL of the SCS, (a) represents all
811 the data excepting the measurements in the PRE; (b) represents all the data. The data shown are
812 the mean and standard error.

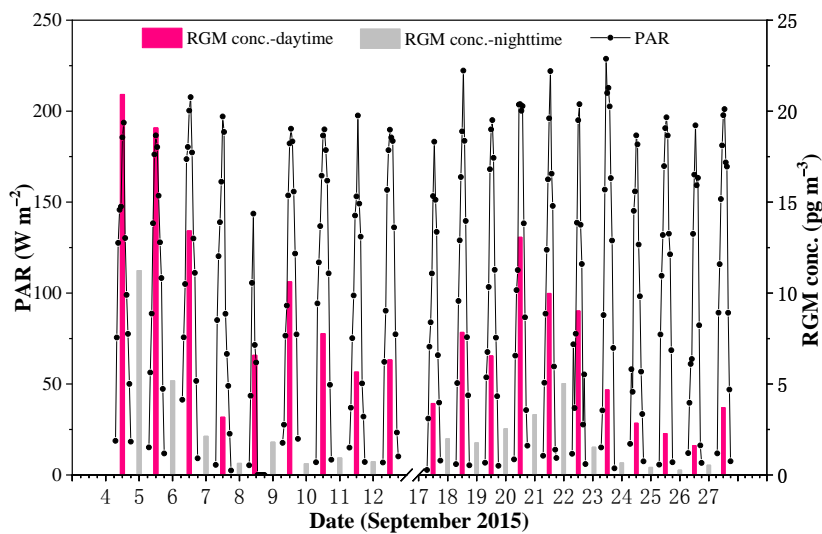
813



814

815 **Figure 6.** Diurnal variation of GEM concentration (mean \pm SD) over the SCS.

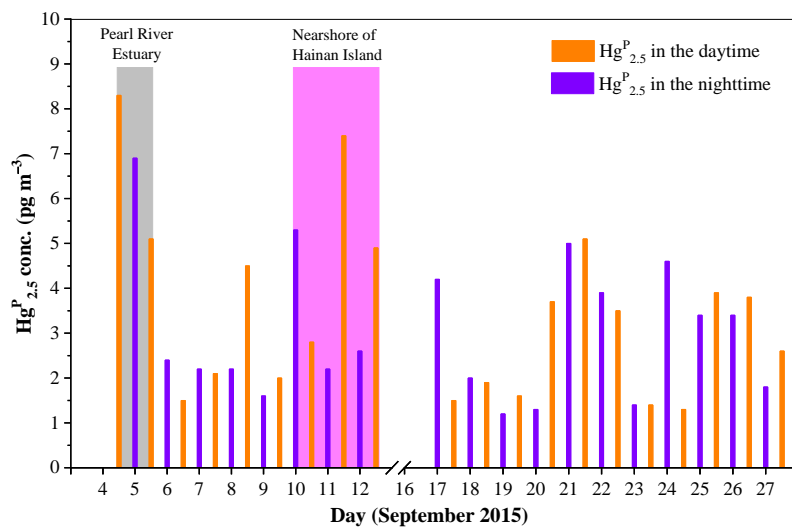
816



817

818 **Figure 7.** Daily variation of RGM concentration over the SCS.

819



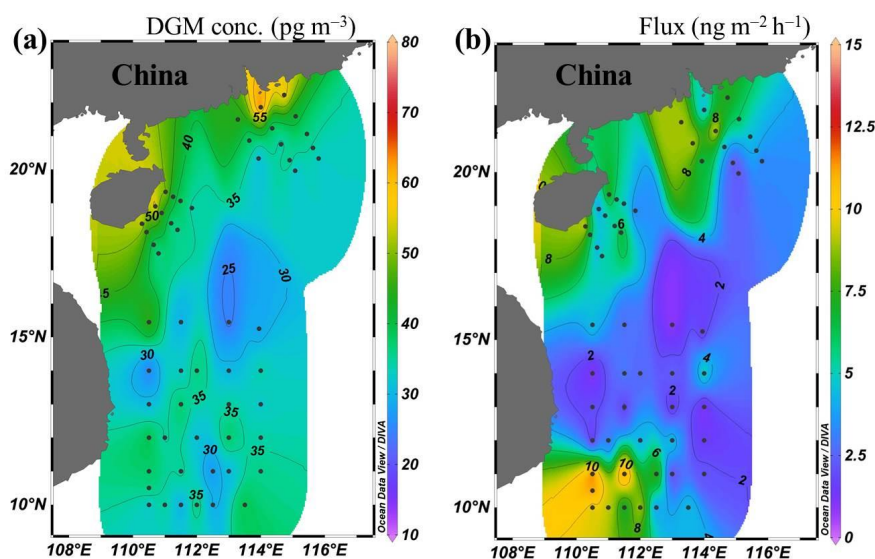
820

821 **Figure 8.** Daily variation of $\text{Hg}^{\text{P}}_{2.5}$ in the MBL of the SCS. The light gray area represents the data

822 in the PRE, while the light magenta area represents the data in the nearshore area of the Hainan

823 Island.

824



825

826 **Figure 9.** Spatial distributions of DGM (a) and sea-air exchange flux of Hg^0 (b) in the SCS.

827

828 **Table 1.** The GEM, $\text{Hg}^{\text{P}}_{2.5}$ and RGM concentrations in this study and other literature.

Location	Classification	Sampling time	GEM (ng m^{-3})	$\text{Hg}^{\text{P}}_{2.5}$ (pg m^{-3})	RGM (pg m^{-3})	Reference	
China	SCS	Sea	2015	1.52 ± 0.32	3.2 ± 1.8	6.1 ± 5.8	This study
	BS and YS	Sea	2014 (Spring)	2.03 ± 0.72	11.3 ± 18.5	2.5 ± 1.7	Wang et al., 2016a, b
	BS and YS	Sea	2014 (Fall)	2.09 ± 1.58	9.0 ± 9.0	4.3 ± 2.5	Wang et al., 2016a, b
	YS	Sea	2010 (Summer)	2.61 ± 0.50	NA ^a	NA	Ci et al., 2011
	YS	Sea	2012 (Spring)	1.86 ± 0.40	NA	NA	Ci et al., 2015
	YS	Sea	2012 (Fall)	1.84 ± 0.50	NA	NA	Ci et al., 2015
	ECS	Sea	2013 (Summer)	1.61 ± 0.32	NA	NA	Wang et al., 2016c
	ECS	Sea	2013 (Fall)	2.20 ± 0.58	NA	NA	Wang et al., 2016c
	Northern SCS	Sea	2007	2.62 ± 1.13	NA	NA	Fu et al., 2010
	Northern SCS	Sea	2003–2005	2.8–5.7	NA	NA	Tseng et al., 2012
	Nam Co	lake	2014–2015	0.95 ± 0.37	0.85 ± 2.91	49.0 ± 60.3	de Foy et al., 2016
	Xiamen	Coastal urban	2012–2013	3.50	61.05	174.41	Xu et al., 2015
Japan	Okinawa Island	Ocean	2004	2.04 ± 0.38	3.0 ± 2.5	4.5 ± 5.4	Chand et al., 2008
Korea	Seoul	Urban	2005–2006	3.22 ± 2.10	23.9 ± 19.6	27.2 ± 19.3	Kim et al., 2009
USA	Weeks Bay	Coast	2005–2006	1.6 ± 0.3	2.7 ± 3.4	4.0 ± 7.5	Engle et al., 2008
Canada	Ontario Lake	Remote area	2005–2006	1.57 ± 0.22	4.42 ± 3.67	0.99 ± 1.89	Cheng et al., 2012
	Nova Scotia	Coast	2010–2011	1.67 ± 1.01	2.32 ± 3.09	2.07 ± 3.35	Cheng et al., 2013
	Nova Scotia	Coast-rural	2010–2011	1.38 ± 0.20	3.5 ± 4.5	0.4 ± 1.0	Cheng et al., 2014
Australia	ATARS ^b	Coast	2014–2015	0.95 ± 0.12	NA	NA	Howard et al., 2017
South-west India Ocean	Ocean	2007	1.24 ± 0.06	NA	NA	Witt et al., 2010	
North Atlantic Ocean	Ocean	2003	1.63 ± 0.08	NA	5.9 ± 4.9	Laurier et al., 2007	
West Atlantic Ocean	Ocean	2008–2010	1.4–1.5	NA	NA	Soerensen et al., 2013	
North Pacific Ocean	Ocean	2002	2.5	NA	9.5	Laurier et al., 2003	
Pacific Ocean	Ocean	2011	1.15–1.32	NA	NA	Soerensen et al., 2014	
Mediterranean Sea	Sea	2000	1.9 ± 1.0	NA	7.9	Sprovieri et al., 2003	
Global Ocean	Ocean	2006–2007	1.53 ± 0.58	NA	3.1 ± 11.0	Soerensen et al., 2010a	
Adriatic Sea	Ocean	2004	1.6 ± 0.4	4.5 ± 8.0	6.7 ± 11.7	Sprovieri and Pirrone, 2008	
Amsterdam Island	Ocean	2012–2013	1.03 ± 0.08	0.67	0.34	Angot et al., 2014	

829 ^a NA: No data available.

830 ^b ATARS: Australian Tropical Atmospheric Research Station.



831 **Table 2.** Correlation coefficients for speciated atmospheric Hg and meteorological parameters (one asterisk

832 denotes significant correlation in $p < 0.05$, double asterisks denotes significant correlation in $p < 0.01$).

Speciation	GEM		RGM		Hg ^p _{2.5}		Wind speed		Air temperature		RH		PAR	
	<i>p</i>	<i>r</i>	<i>p</i>	<i>r</i>	<i>p</i>	<i>r</i>	<i>p</i>	<i>r</i>	<i>p</i>	<i>r</i>	<i>p</i>	<i>r</i>	<i>p</i>	<i>r</i>
RGM	0.069	0.294			< 0.01	0.453**	0.123	-0.251	0.053	0.313	0.065	-0.299	< 0.01	0.638**
Hg ^p _{2.5}	< 0.01	0.539**	< 0.01	0.489**			0.037	-0.335*	0.621	0.082	0.434	-0.129	0.432	0.130

833